Arabian Journal of Chemistry (2021) **14**, 103066

King Saud University

Arabian Journal of Chemistry

www.ksu.edu.sa
www.sciencedirect.com

ORIGINAL ARTICLE

Chemical, microbial and biological studies on fresh mango juice in presence of nanoparticles of zirconium molybdate embedded chitosan and alginate

Ahmed A. Aly [a], Ismail M. Ali [b], M. Khalil [b], Ahmed M. Hameed [c,*], Abdulmajeed F. Alrefaei [g], Hussain Alessa [c], Alia Abdulaziz Alfi [c], M.A.A. Hassan [d], M.Y. Abo El-Naga [d], Aml A. Hegazy [d], M.M. Rabie [e], M.S. Ammar [f]

[a] *Home Economics Department, Faculty of Specific Education, Benha University, Egypt*
[b] *Hot Labs. Center, Atomic Energy Authority, P. No. 13759 Cairo, Egypt*
[c] *Department of Chemistry, Faculty of Applied Sciences, Umm Al-Qura University, 21955 Makkah, Saudi Arabia*
[d] *Food Sci. Dept., Faculty of Agriculture. Ain Shams University, Egypt*
[e] *Food Industries Dept., Faculty of Agriculture. Mansoura University, Egypt*
[f] *Food Sci. and Technology Dept., Faculty of Agriculture, Al-Azhar University, Egypt*
[g] *Department of Biology, Jamoum university college, Umm Al-Qura University, 21955 Makkah, Saudi Arabia*

Received 30 December 2020; accepted 4 February 2021
Available online 18 February 2021

KEYWORDS

Nanoparticles;
Zirconium molybdate;
Chitosan;
Alginate;
Composite;
Antimicrobial;
Biological;
Mango juice

Abstract New antimicrobial nancomposites based $Zr(MoO_4)_2{\cdot}3H_2O$ was developed through the sonication impregnation with natural polymers (chitosan and alginate). These materials were physiochemical characterized using X-ray powder diffraction technique (XRD), SEM, FTIR spectra and DTA/TG thermal analysis. The XRD results confirmed the amorphous properties of Zr $(MoO_4)_2$ which hold semicrystalline nature after impregnation with the polysaccharides. The data have shown that these composites reveal high thermal and chemical stabilities and microstructure surface coated with nanoscale units. Doping of such nanoparticles (($Zr(MoO_4)_2$, $Zr(MoO_4)_2$/chitosan and $Zr(MoO_4)_2$/alginate)) into fresh mango juice in 0.01% compared to sodium benzoate additive and control sample demonstrate a superior antimicrobial properties. The data revealed that

* Corresponding author at: Department of Analytical Chemistry – Faculty of Applied Science, Umm Al-Qura University – Makkah, Saudi Arabia.
E-mail addresses: ahmed.abdelfatah@fsed.bu.edu.eg (A.A. Aly), amhameed@uqu.edu.sa (A.M. Hameed).
Peer review under responsibility of King Saud University.

Production and hosting by Elsevier

https://doi.org/10.1016/j.arabjc.2021.103066
1878-5352 © 2021 The Author(s). Published by Elsevier B.V. on behalf of King Saud University.
This is an open access article under the CC BY-NC-ND license (http://creativecommons.org/licenses/by-nc-nd/4.0/).

the best treatment in retardation of the microbial load (total bacterial, psychrophilic bacteria, spore-forming bacteria, total molds, and yeasts counts) was detected in fresh mango juice samples prepared using 0.01% additives are in the following order; ZrMo/chitosan > ZrMo/alg > ZrMo ≫ sodium benzoate additive. It was observed no any undesirable changes in biological characters (body weight, relative organs weigh, serum cholesterol, triglycerides, HDL, LDL, urea, creatinine, GPT and GOT) of albino rats received a fresh meal of mango juice doped with these nanoparticles. This result confirmed the safe application and positive impact of the modified nanoparticles in fresh mango juice to extend shelf life keeping the quality of their sensory properties.

© 2021 The Author(s). Published by Elsevier B.V. on behalf of King Saud University. This is an open access article under the CC BY-NC-ND license (http://creativecommons.org/licenses/by-nc-nd/4.0/).

1. Introduction

Advanced composite materials are gaining popularity for the past few years due to their promising physicochemical properties. Also, the composites possess better mechanical and radiation stability in addition to enhance reproducibility. Such materials have been designed not only to overcome the properties limitations of individual constituents but also depend on the morphology and interfacial characteristics. Recently, composites such as poly-o-toludine zirconium (IV)tungestophosphate, graphene oxide/chitosan/ zirconium phosphate/silicate, chitosan/Ag/MoS_2, alginate/chitosan-silver, cellulose/sodium alginate hydrogel beads etc., have been prepared while maintaining the better properties of their ingredients (Zhu et al., 2020; Ali et al., 2020, Zakaria et al., 2016, Sharma et al., 2012, Venkatesan et al., 2017; Hu et al., 2018). On the other hand, several metal ions and metal oxides which in combination with alginate and chitosan have been reported to exhibit marked antimicrobial action against various microbial strains (Wahid et al., 2017b). Therefore, these materials have attracted great interest of the healthcare and environmental industries. Many of these studies have been carried out to explain the antimicrobial mechanism and efficacy of metals and metal oxide nanoparticles. In this concern, facile fabrication of moldable antibacterial carboxymethyl chitosan supramolecular hydrogels cross-linked by metal ions (Ag^+, Cu^{2+} and Zn^{2+}) complexation (Wahid et al., 2017a) was reported. The hydrogels cross-linked by metal ions can enhance the antimicrobial activity, that a faster hydrogelation could be achieved, that the hydrogels may show self-healing properties and that the resultant hydrogels may show viscoelasticity (Wahid et al., 2017b). A new method for producing of composite sponges with a pronounced antimicrobial effect based on such biological polymers as alginate and chitosan with the addition of silver nanoparticles has been proposed (Gordienko et al., 2020).

These hybrid materials showed improvements in some properties such as ion exchange properties, selectivity for heavy metals and antimicrobial activity. In this regard, literature revealed that nanocomposites have enhanced subsurface transport characteristics and reactivity. Nowadays, nanocomposites have been synthesized to act as better remedies for water contaminants such as toxic metals, waterborne bacteria and municipal, industrial and agricultural processes (Zhu et al., 2020; Ali et al., 2020, Zakaria et al., 2016, Sharma et al., 2012, Venkatesan et al., 2017; Hu et al., 2018). Among various classes of inorganic materials, the synthetic tetravalent metal acid salts (TMAS) are of high interest due to their unique stability and selectivity towards metal ions. $M(HXO_4)_2{\cdot}nH_2O$ is the general formula of TMAS, M = Zr (IV), Sn(IV), Ce(IV), Ti(IV), etc., and X = Mo, P, As, Sb, W, etc. (Zhang et al., 2015). The presence of structural hydroxyl protons in TMAS is responsible for their ion-exchange characters. TMA salts have a variety of applications in different fields depending on the properties. Among TMAS, $ZrMo_2O_8$ has concerned severe importance due to its advanced applications in negative thermal expansion materials (Gallington et al., 2013), ions separation (Clearfield and Blessing, 1972), and optical material (Blasse and Dirksen 1987), catalyst in formaldehyde and propylene preparation and in photcatalytic degradation of organic dyes (Liu et al., 2003; Chen et al., 2001; Sahoo et al., 2009). Also, $ZrMo_2O_8$ gel has been used in medical applications as source for the production of ^{99m}Tc (^{99m}Technetium) isotope from the radioactive decay of activated molybdenum (Clearfield and Blessing, 1972; Monroy-Guzmán et al., 2003). Recently, a hybrid zirconium molybdate in nanosize impregnated within a commercial macroporous anion exchange resin was successfully fabricated for efficient separation of phosphate (Bui et al., 2018).

Food corruption and spoilage produced by food-borne pathogens and microorganisms is a serious problem. Thus, the request for antibacterial additives in food safety is growing. Antibacterial agents are a group of substances that fight against pathogenic microorganisms. Thus, by killing or resistance the metabolic activity of bacteria, their negative effect in the biological system will be reduced. Of which methods to produce materials having antibacterial efficiency, the surface modulation process where the surface can doped with antibacterial inorganic nanoparticles or organic agents. Chitosan (CS) is one of a natural materials that displays a slightly of antibacterial character and superior biocompatibility (Chen et al., 2016, Cheng et al., 2018). The antibacterial power of CS is due to its excess positive charge groups (Gan et al., 2019), and it can be efficient to lower cell-toxicity comes from complexion with the metal ions (Li et al., 2016) Due to their unique physicochemical and biological properties, both chitosan and alginate have wide applications in food industry, agriculture, pharmacy and medicine owing to its biocompatibility and biodegradability. Chitosan is a cationic hydrophilic natural polysaccharide with high density of positive charge. Chitosan is a copolymer of N-acetyl glucosamine and glucosamine unit produced from alkaline deacetylation of chitin. It (Patiño-Ruiz et al., 2020) has been widespread utilize in biological and biomedical purpose. In addition, alginate is a naturally occurring anionic polysaccharide that is mainly composed of L-guluronic and D-mannuronic acids in different ratios Patiño-Ruiz et al. (2020). In aqueous solutions, at pH around 4–5.5 the amine groups on chitosan became easily positively

charged. Alginate, on the other hand, dissolved in a neutral pH solution where the carboxylate groups were negatively charged. In aqueous solutions with pH around 5.2 chitosan amino groups interacted with alginate carboxylate groups to form the hydrogel. The pH of the alginate solution was ≈6.5, and the pH of the chitosan chloride solution was ≈4.0 after the dissolution. These pHs ensured that the alginate was fully deprotonated and that the chitosan was fully protonated (Kulig et al., 2016, Sæther et al., 2008). The majority of antimicrobial composite materials have obtained by blending substance that kills or inhibits the growth of microorganisms (antimicrobial agent). Copper is well known as one of this family, for a long time ago (Tamayo et al., 2016) Yin et al. reported that Cu^{2+}/carboxymethyl chitosan/poly vinyl alcohol blend composite films can be obtained with good antibacterial efficiency (Yin et al., 2018). Cu^{2+} as an essential nutrient is of great interest because of its role in biocatalytic chemical processes as well as the potential antimicrobial effect (Hultberg et al., 1997; Chvapil et al., 1978). Moreover, in 2019 Pogrebnjak et al., studied the synthesis of a nanostructured composite material in the form of a hydrogel and beads based on hydroxyapatite (HA), sodium alginate (Alg) and ZnO microparticles under the influence of microwave irradiation. The mechanism of antimicrobial activity of ZnO crystals in the HA-Alg-ZnO was proposed. The introduction of ZnO into the composite provides slight antimicrobial activity (Pogrebnjak et al., 2019). Also, in 2019 Turlybekuly et al., studied the biocompatibility and antibacterial properties of multiphase nanocomposites materials based on HA-Alg-ZnO (hydroxyapatite sodium alginate-biphasic zinc oxide) and HA-ZnO. The studied composites demonstrate a pronounced antibacterial activity due to the incorporation of ZnO particles into sodium alginate and hydroxyapatite. Both forms of HA-ZnO (suspension) and HA-Alg-ZnO (beads) are biocompatible (Turlybekuly et al., 2019). Cellulose acetate/tin (VI) molybdate (CA-SnMo) was also reported as an antimicrobial nanocomposite (Hultberg et al., 1997). The antibacterial activity of CA-SnMo was examined against Escherichia coli. The results indicated the bacteriostatic nature of the composite (Gupta et al., 2015). Recently, cell culture studies revealed that chitosan/Ag/MoS_2-Ti had no adverse effects on cell life. Moreover, the impregnation with chitosan gain the material positively charged which further enhance the antibacterial character (Zhu et al., 2020). Hence, this system and others like it will be a promising strategy and is urgently required to achieve a high efficiency for antibacterial protection and fills safely and effectively within a concise time. This manuscript was focused to develop novel nontoxic antimicrobial nano composites based $Zr(MoO_4)_2$ with each chitosan and alginate. The developed $Zr(MoO_4)_2$/chitosan and $Zr(MoO_4)_2$/alginate beads were explored for their compositions, thermal stabilities and surface morphologies using different techniques. The materials performance for juice antimicrobial resistance and safe biological applicability was investigated.

2. Experimental

All chemicals used are of analytical grade and used without additional treatment. Mango fruits (*Mangifera indica* L.) were preheated from local market in Egypt.

2.1. Preparation of zirconium molybdate gel (ZrMo)

Zirconium molybdate gel was prepared by application of the gel-precipitation route developed at China (Le, 1993). In a typical procedure, the gel was growth via dispersing MoO_3 in NaOH (2 mol/L). The obtained Na_2MoO_4 solution was neutralized using 2 M HNO_3 until pH ≈ 4.5. This solution is then added in drop wise with vigorous stirring at room temperature to $ZrOCl_2{\cdot}8H_2O$ (20 mg/mL) and heated to 50 °C (Zr/Mo ≈ 0.5) with continuous stirring for 30 min. The colloidal dispersion formed (pH ≈ 1–2) was neutralized using NaOH (2 mol/L), whereas the pH nearly 5. The formed jelly-like white precipitate was separated by filtration and then dried at 105 °C in a drying oven. Finally, the obtained molybdate was ground into fine particles.

2.2. Modification of ZrMo

First; 0.5 g chitosan was dissolved in 10 ml of 2% (w/v) acetic acid solution with magnetic stirring (500 rpm) for about 1 h until the solution became transparent. At the same time, 0.5 g of sodium alginate was added into 10 ml distilled water with continuous stirring to obtain homogeneous sodium alginate suspension. After which, about 10 g of ZrMo was again grinded to microsize (< 50 μm) powder using agate mortar then divided into two equal weights (5 g). Each 5 g immersed in 50 ml of water and ethanol mixture have been subjected to sonication for 1 h to produce a homogenous suspension of each. Then, the prepared solutions of each 0.5 g of chitosan and sodium alginate were added to the above suspensions of ZrMo, respectively. 1 ml of 0.2% of each glutraldehyde and $CaCl_2$ were added as crosslinkers to the above suspensions, respectively with continuous stirring up to gelation the chitosan and sodium alginate complete with formation a solid gel mass in deep yellow homogenized particles. A homogenous gel was produced for each composite. Afterwards, drying at 70 °C for 2 days followed by cracking with double distilled water then washing for many times until the synthesized products are free from any impurities or residual ions and dried in electric oven. Scheme 1 describes the synthesis steps of both ZrMo/chitozan and ZrMo/alginate composites.

2.3. Materials characterization

XRD diffraction patterns are recorded by X-ray diffractometer, XD 610, Shimadzu model, with a nickel filter and Kα Cu radiation (1.54 Å) at 30 kV and 30 mA. The phase stability of the materials was detected using a DT60 thermal analyzer, Shimadzu model, Japan. The measurement carried out up to 600 °C at a heating rate of 15 deg /min under N_2 environment. Function groups of the materials were recorded using a Bomem FTIR spectrometer applying KBr disc technique. The wave number in cm^{-1} was carried at 4000–400 at resolution 4 cm^{-1} and accuracy 1 cm^{-1}. Quantitative elemental analysis was detected via a Phillips X-ray fluorescence model PW 2400 spectrometer applying the pressed technique. Morphologies of the composites were examined by SEM Model Quanta 250 FEG (Field Emission Gun) equipped with energy dispersive X-ray (EDX) with accelerating voltage 30 K.V.

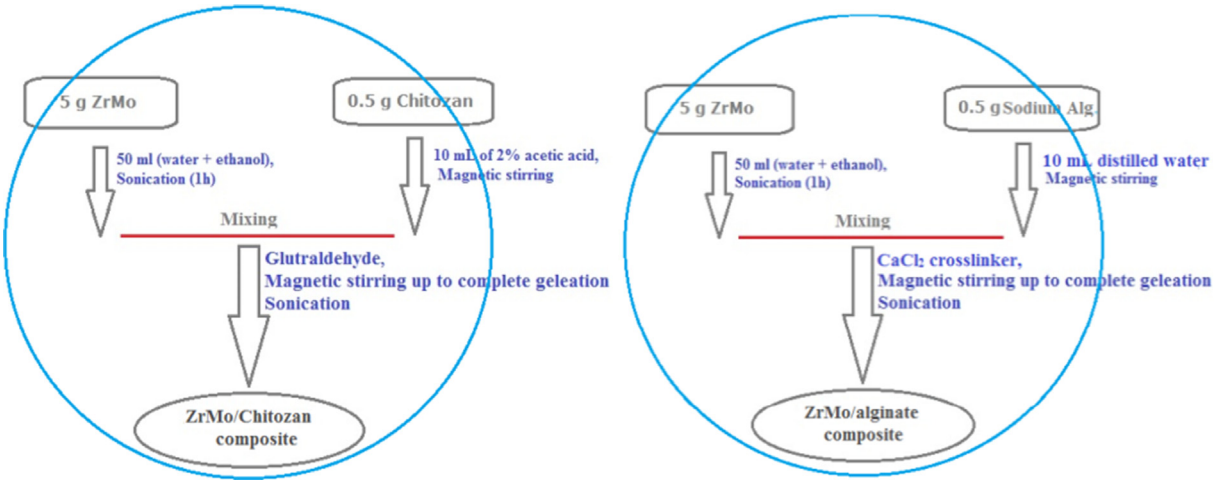

Scheme 1 The synthesis steps of ZrMo/chitozan and ZrMo/alginate composites.

2.4. Fresh mango juice samples preparation

Fresh mango juice samples prepared according to the method of (Pan, et al., 2021), with minor modification as follow, the seeds and peels were separated from mango fruits then the fruit pulp cut to small pieces and mixed in a juicer for five minutes. Fresh mango juice collected and kept in glass bottles in refrigerator at 4 ± 2 °C after adding sodium benzoate, ZrMo, ZrMo/Chitosan and ZrMo/Alg with percentage 0.01% to obtain four groups of fresh juice treated samples in compared with the fifth control group (without any additives). Fresh mango juice treatments were evaluated immediately after preparation and during storage period (10 days) each 2 days at cooling (4 ± 2 °C).

2.5. Organoleptic properties

Sensory attributes (taste, odor, and color) of fresh mango juice samples scored according to score card suggested by Aly et al. (2020) by staff members of the Home Economics Department, Faculty of Specific Education, Benha Univ., Egypt, after 2 h hardening at 4 ± 1 °C were organoleptically examined by 10 semi-trained panelists.

2.6. Microbiological analyses

Total bacterial count, psychrophilic bacteria, spore forming bacteria, moulds & yeasts counts determination were carried out as methods described by Aly et al. (2020).

2.7. Biological evaluation

2.7.1. Experimental animals

A total of twenty-five of male albino rats weighting 182–183 g were divided to five groups (each group consists of five rats). The rats were kept under normal laboratory conditions in the animal's house of Agricultural Research Center, Egypt, for three days before the initiation of the experiment. Then groups of rats were housed in stainless steel cages at raised shelves during the experimental period, which lasted for 4 weeks. They were accessed to water and fed on experimental diets, which prepared according to standard method of AOAC (1995) fresh mango juice samples under investigation added daily to diets with 15%.

2.7.2. Experimental procedure and measurements:

2.7.2.1. Tissue collection. At the termination of the 4 weeks experimental period, the rats were fasted for 6 hr., then weighed and decapitated, the tissues (liver, kidney, spleen and heart) were separated and cleaned from adherent tissues and weighed at once. Relative tissue weights were expressed as body weight.

2.7.2.2. Blood and serum samples collection. The blood samples were collected from the retro orbital plexus vein in dry clean centrifuge tubes (15 ml.) using a fine capillary glass tubing according to the procedure described by Schermer and Winsen (1967). The tubes were kept for about half an hr. at room temperature to allow blood to clot, then the tubes were centrifuged at 3000 rpm for 10 min. and the clear serum was separated and stored in the deep freezer at stored at −10 °C for subsequent biochemical analysis.

2.7.3. Biochemical analysis

2.7.3.1. Serum total lipids. The total lipids concentration of blood serum was determined according to the method described by Frings et al. (1972).

2.7.3.2. Determination of total cholesterol. Total cholesterol was determined according to the method of Allain et al. (1974).

2.7.3.3. Determination of plasma transaminase activities and aspartate aminotransferase (GPT and GOT). Serum Alanine aminotransferase GPT (ALT) and aspartate transaminase GOT (AST) were determined calorimetrically according to the method described by Reitman and Frankel (1957).

2.7.3.4. Determination of creatinine. Creatinine in a basic picrate solution forms a colored complex. The D-extension at predetermined times during conversion is proportion to the concentration of creatinine in the sample according to the method described by Thammitiyagodage et al. (2020).

2.7.3.5. Determination of urea. Urea content of the serum sample was determined as method estimated by Fawcett and Scott (1960).

2.7.3.6. Determination of High Density Lipoprotein-cholesterol. High Density Lipoprotein-cholesterol (HDL-C) were determined according to the methods Salè et al. (1984) by an enzymatic colorimetric method.

2.7.3.7. Determination of Low-Density Lipoprotein-cholesterol. Low- Density Lipoprotein-cholesterol (LDL-C) was calculated using methods Friedewald et al. (1972) by the formula LDL-C = TC–HDL-C–(TG/5).

2.8. Statistical analysis

Using SPSS software (version 20) the data were analyzed statistically using one-way analysis of variance $P \leq 0.05$. The results were expressed as mean ± SD as reported by Ismail et al. (2020).

3. Results and discussion

A prominent place can be occupied by salts of polyvalent metal acids after impregnation with natural polymer, which may be used for the first time as antimicrobial materials. In this study, ZrMo was prepared and modified through natural polymer sonochemically impregnation. A cross-linkage gelation of chitosan and alginate polymers was performed in the presence of ZrMo. Scheme 2 represents the structure of the ZrMo in the developed composites.

3.1. FT-IR spectroscopy

The IR spectrum of the zirconium molybdate (Fig. 1a) contains a strong broadening band at 3424 cm^{-1}, can is assigned to OH stretching frequency of water molecules involved in intermolecular hydrogen bonds. Also, a strong peak at 1627.5 cm^{-1} may be assigned to H_2O molecules. Other bands

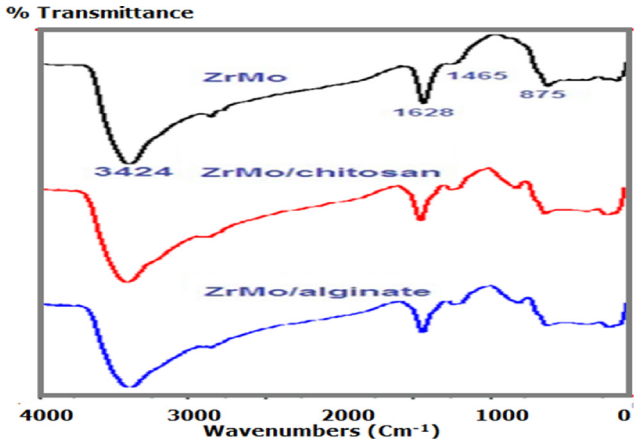

Fig. 1 IR spectra of ZrMo, ZrMo/chitosan and ZrMO/alginate.

detected around 600 cm^{-1} are assigned to the M—O interactions. The spectrum of ZrMo (Fig. 1a) shows also strong peak at 875 cm^{-1} indicating the presence of molybdate group (Bui, Hong and Yoon 2018). Fife bands appear at 773, 643, 530, 443, 426w cm^{-1} indicated to super positions of metal–oxygen stretching (Zr—O and Mo—O) and aqua wagging, twisting, and rocking modes of this basic ZrMo are observed.

On the other hand Fig. 1 (b and c) shows the IR spectra of the ZrMo after incorporation with chitosan and alginate. The spectra reveal new peaks at 1449.5, 1400, 1047 s cm^{-1} and at 1428, and 1042 m cm^{-1} characteristic the presence of chitosan and alginate in composition of ZrMo/chitosan and ZrMo/alginate, respectively. The new spectra as well as the deep yellowish colors confirm the formation of both composites.

3.2. Thermal analysis of materials

Fig. 2(a–c) shows the DTA/TG thermogram of ZrMo, ZrMo/chitosan and ZrMo/alginate, respectively. Fig. 2a demonstrates an irreversible endothermic peak at ≈132 °C, corresponding to free water dehydration (13.3%). The mass

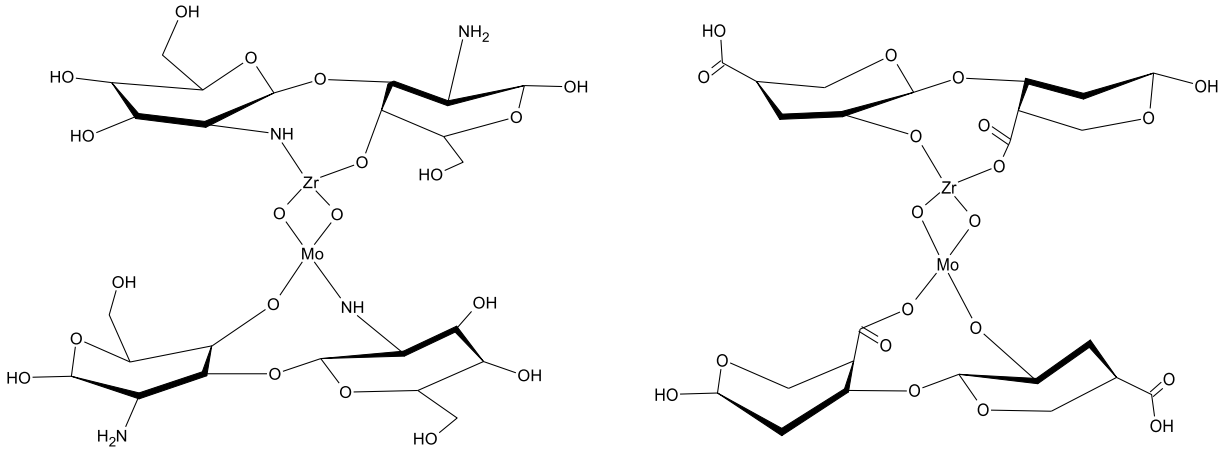

Scheme 2 Structure of ZrMo/chitosan (a) and ZrMO/alginate (b).

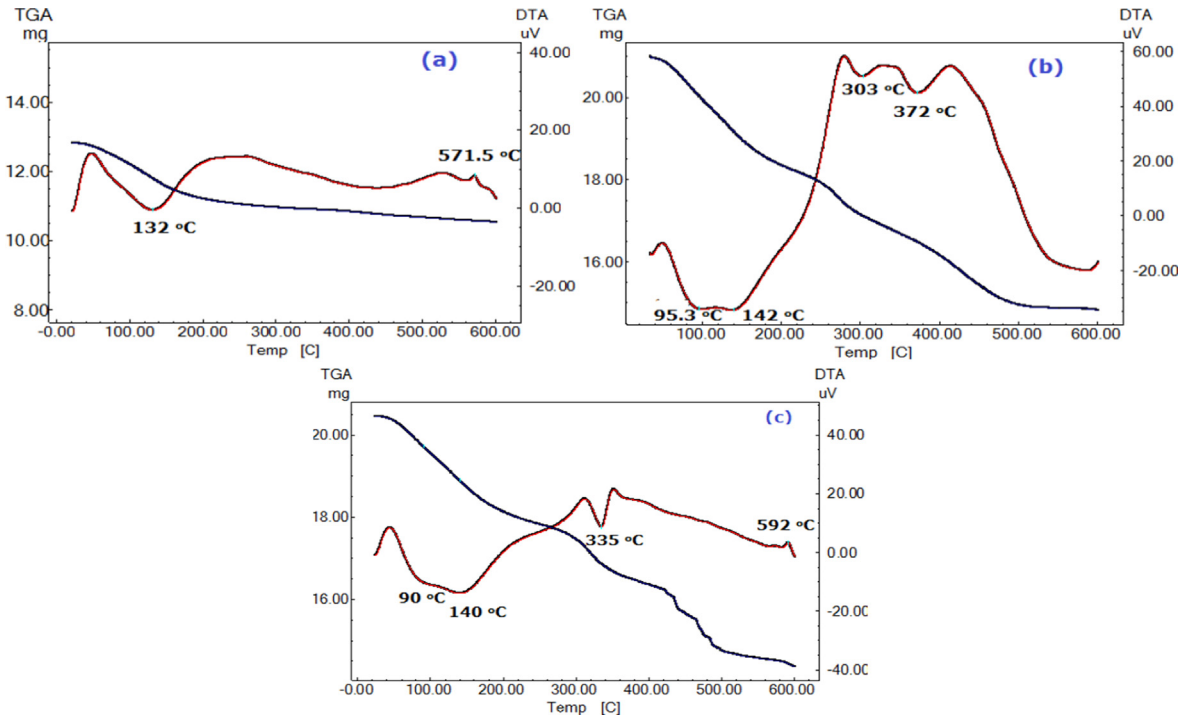

Fig. 2 DTA/TG thermal analyses of ZrMo (a), ZrMo/chitosan (b) and ZrMo/alginate (c).

loss continued up to 600 °C, due to crystalline water dehydration (4.4%). An exothermic change appeared at 571 °C may correspond to ZrMo phase transformation into zirconia and molybdenum oxide (Monroy-Guzmán et al., 2003; El-Gammal et al., 2015). The absence of the peak corresponding to the transformation to oxides in case of ZrMo/chitosan thermogram (Fig. 2(b)) cannot be considered a disappearing of this change, but it may be delayed to a range beyond 600 °C, i.e. to a higher temperature range (>600 °C). This may be demonstrated by the delay of that summit in case of ZrMO/alginate to 592 °C. The overall water content obtained from TGA measurements was found to be 17.7 wt% which is nearly the same as that obtained by El-Gammal et al. (2015). Fig. 2b describes 4 simultaneous mass changes (7.0, 6.5, 6.1, 9.4% to give total loss = 29.0%) corresponding to the endothermic changes at T_{max} = 95.3, 140.3, 303.25 and 372.8 °C. The first and second peaks correspond to removal of surface and interstitial water molecules while the later peaks correspond to the polymer degradation. Fig. 3c shows 3 endothermic peaks at 90, 140, and 335 °C corresponding to the 5.6, 6.75, 7.66% mass loss while there are a forth mass loss ≈9.22% not reveal any DTA peak. Also, at 492 °C an exothermic peak was reported can be attributed to excess degradation at higher temperature. The total mass change ≈ 29.5%. Therefore, similarity in thermal degradation for both composites was observed. This low thermal stability with high mass loss (29.5%) compared to ZrMo (17.7%) confirms presence of chitosan and alginate in the chemical structure of the new composites. Also, the large difference in mass loss % between the ZrMo and composites that not compatible with the initial mass of the two polymers may due to the higher water content of composites (hydrogel characters) compared to the inorganic species. The number of mole of water (n) of each nanocomposite was calculated applying Albert model (Ali, 2010): 18n = x (M + 18n)/100, where x is the water content %, and M + 18n is the molecular weight of the composite material.

3.3. X-ray diffraction

The XRD patterns were investigated to find the crystallinity of the nanocomposite materials. Analysis of ZrMo is shown in Fig. 3 a; it shows that the sample has an amorphous structure. An improvement to semicrystalline nature was detected after modification with chitosan or alginate (Fig. 3b and c). No peak characteristic for each chitosan or alginate was detected due to their low concentrations in the composites.

3.4. SEM studies

Fig. 4a shows a microsize smoothed particles like layers of Sea Sand covered with a little of nanoparticles. Fig. 4b shows bright lighting porous clusters of cloud shape covered with nanoparticle. Fig. 4c shows rough porous material carry some of nanoparticles.

3.5. Elemental analysis

However the EDX analysis is a semiquantitative tool for materials investigation, it was used here for conforming the formation of the prepared materials. Fig. 5(a and b) shows the EDX spectra of both composites ZrMo/chitosan and ZrMo/alginate, respectively. It can be seen that presence of Mo and Zr with the majority of molybdenum in the products confirming the proposed formula of material $Zr(MoO_4)_2$. Further, the presence of nitrogen may be confirming the formation of ZrMo/chitosan while presence of Ca^{2+} cannot directly indicate the presence of alginate, because alginate macromolecules

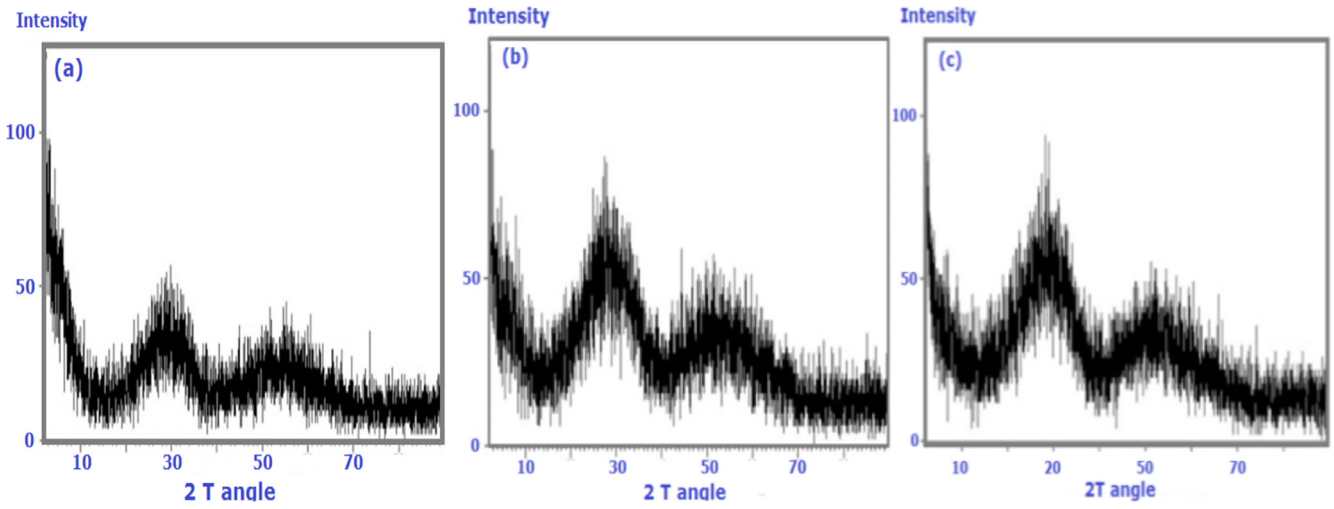

Fig. 3 X-ray diffraction patterns of ZrMo, ZrMo/chitosan and ZrMO/alginate.

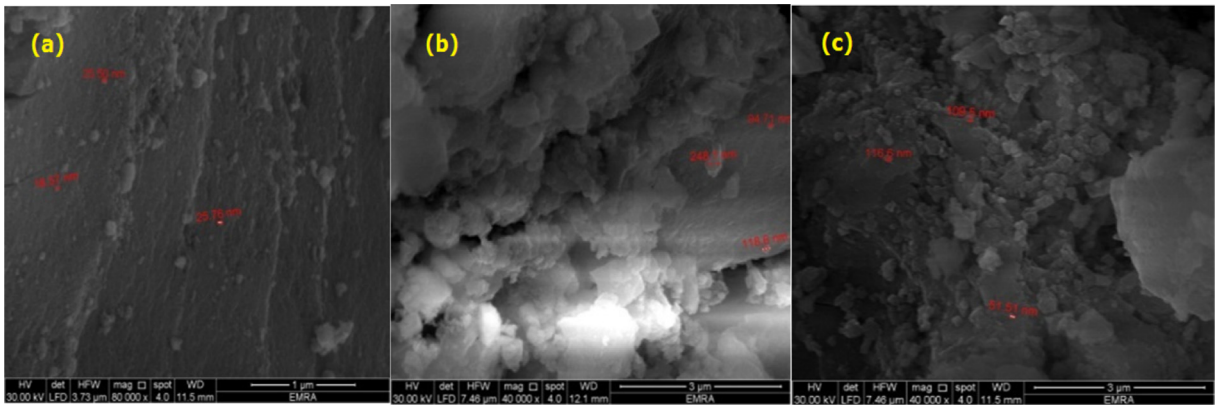

Fig. 4 Scanning electron microscopy (SEM) images of the as-synthesized ZrMo, ZrMo/chitosan and ZrMO/alginate at 80,000 magnifications.

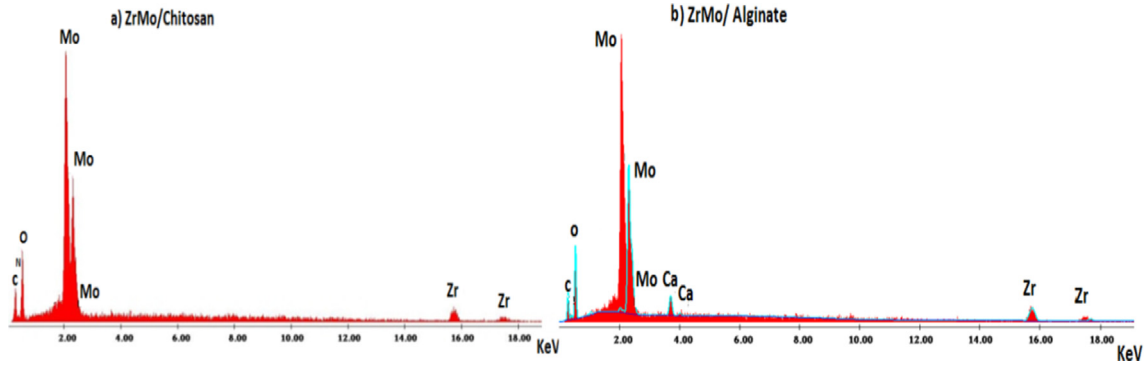

Fig. 5 Energy dispersive X-ray analyses (EDX) of ZrMo/chitosan and ZrMO/alginate.

do not contain calcium. The calcium present in the EDX spectrum may be belongs to calcium chloride. Ca^{2+} may be entered the structure of the composite containing alginate molecules as a cross-linker or by surface adsorption. Based on the above discussion, $Zr(MoO_4)_2{\cdot}3H_2O$ has been obtained.

3.6. Sensory evaluation of fresh mango juice during cold storage

Table 1 showed the sensory properties of fresh mango juice as affected by sodium benzoate, ZrMo, ZrMo/Chitosan and ZrMo/AlG additives during cold storage (4 ± 1 °C). The

results showed that no a significant ($P > 0.05$) difference was found between the fresh mango juice samples under investigation. It could be noticed the sensory attributes (taste, odor, and color) of fresh mango juice samples prepared with 0.01% ZrMo/AlG and ZrMo/Chitosan were rejected after 10 and 8 days for 0.01% ZrMo and 0.01% Sodium benzoate compared to the control samples which were rejected on the 6th day of cold storage.

Hence, fresh mango juice samples prepared with ZrMo/AlG and ZrMo/Chitosan were scored the best treatment, compared to the other samples. This may be due to the effects of this materials and their improve on some properties such as ion exchange properties, selectivity for heavy metals and antimicrobial activity (Zhu et al., 2020; Ali et al., 2020; Zakaria et al., 2016; Sharma et al., 2012; Venkatesan et al., 2017; Hu et al., 2018) who revealed that nanocomposites (graphene oxide/chitosan/zirconium phosphate/silicate, chitosan/Ag/MoS_2, alginate/chitosan-silver) have enhanced subsurface transport characteristics and reactivity. Nowadays, nanocomposites have been synthesized to act as better remedies for water contaminants such as toxic metals, waterborne bacteria and municipal, industrial and agricultural processes.

3.7. Microbial evaluation

Bacterial aspects of fresh mango juice samples and the effects of sodium benzoate, ZrMo, ZrMo/Chitosan and ZrMo/AlG during storage at 4 ± 1 °C were enumerated and presented in Table 2. The initial counts of total bacterial, psychrophilic bacteria, spore forming bacteria, total molds and yeasts counts of control fresh mango juice samples were high counts (7.7×10^3, 2.5×10^2, 3.9×10^2 and 4.0×10^3 CFU/ml, respectively) while addition of sodium benzoate, ZrMo, ZrMo/Chitosan and ZrMo/AlG (0.01%) to fresh mango juice formulas lowered the counts of microbial load. In addition, the best treatments to retardation the microbial loud were noticed in fresh mango juice samples which were prepared using 0.01% ZrMo/Chitosan and 0.01% ZrMo/AlG additive followed by that prepared by using 0.01% ZrMo and 0.01% Sodium benzoate additive. Furthermore, the addition of 0.01% ZrMo/Chitosan and 0.01% ZrMo/AlG extended shelf-life of fresh mango juice to 8 days, respectively followed by 6 days for 0.01% ZrMo and0.01% Sodium benzoate additive compare with 4 days for the control sample. These data confirmed by those reported with (Zhu et al., 2020; Ali et al., 2020; Zakaria et al., 2016; Sharma et al., 2012, Venkatesan et al., 2017; Hu et al., 2018) who reported that hybrid materials (poly-o-toludine zirconium (IV) tungestophosphate, graphene oxide/chitosan/ zirconium phosphate/silicate, chitosan/Ag/MoS_2, alginate/chitosan-silver, cellulose/sodium alginate hydrogel beads, etc.,) improve some properties such as ion exchange properties, selectivity for heavy metals and antimicrobial activity. The main reason for the antimicrobial activity of metal-containing composites is the formation of reactive oxygenated species (ROS), which lead to damage to the cell membrane and bacterial cell death and thus extended shelf life of fresh juice (Pogrebnjak et al., 2019, Turlybekuly et al., 2019).

Table 1 Sensory properties of fresh mango juice samples as affected by sodium benzoate, ZrMo, ZrMo/chitosan and ZrMo/Alginate during cold storage (4 ± 1 °C).

Sensory properties	Storage (Days)	Fresh mango juice samples				
		Control	Fresh mango juice with 0.01% Sodium benzoate	Fresh mango juice with 0.01% ZrMo	Fresh mango juice with 0.01% ZrMo/Chit.	Fresh mango juice with 0.01% ZrMo/Alg.
Taste	Zero time	9.52 ± 0.12	9.41 ± 0.22	9.56 ± 0.27	9.57 ± 0.40	9.59 ± 0.42
	2	9.17 a ± 0.27	9.26 ± 0.28	9.45 ± 0.08	9.31 ± 0.20	9.45 ± 0.31
	4	8.54 a ± 0.18	8.64 ± 0.12	8.34 ± 0.15	8.42 ± 0.42	8.64 ± 0.24
	6	®	7.1 ± 0.17	7.2 ± 0.15	7.42 ± 0.14	7.85 ± 0.31
	8		®	®	7.31 ± 0.24	7.41 ± 0.02
	10				®	®
Flavor	Zero time	9.05 ± 0.42	9.01 ± 0.3	9.03 ± 0.42	9.35 ± 0.34	9.41 ± 0.14
	2	9.01 ± 0.32	9.00 ± 0.08	9.00 ± 0.31	9.01 ± 0.12	9.03 ± 0.45
	4	8.75 ± 0.52	8.74 ± 0.42	8.76 ± 0.45	8.75 ± 0.35	8.97 ± 0.35
	6	®	7.03 ± 0.51	7.24 ± 0.16	7.73 ± 0.44	7.98 ± 0.21
	8		®	®	7.34 ± 0.25	7.42 ± 0.32
	10				®	®
Color	Zero time	9.34 ± 0.62	9.71 ± 0.37	9.32 ± 0.42	9.85 ± 0.44	9.54 ± 0.55
	2	9.31 ± 0.42	9.40 ± 0.08	9.50 ± 0.41	9.41 ± 0.62	9.33 ± 0.34
	4	8.65 ± 0.32	8.69 ± 0.52	8.76 ± 0.43	8.67 ± 0.02	8.95 ± 0.61
	6	®	7.64 ± 0.35	7.45 ± 0.61	7.63 ± 0.02	7.74 ± 0.34
	8		®	®	7.54 ± 0.54	7.34 ± 0. + 65
	10				®	®

®: At these point samples were rejected.

Table 2 Microbial load of fresh mango juice samples as affected by sodium benzoate, ZrMo, ZrMo/Chitosan and ZrMo/AlG during cold storage (4 ± 1 °C).

Microbiological parameters	Storage period (Days)	Microbial counts of fresh mango juice samples (Cfu/g)				
		Control	Fresh mango juice with 0.01% Sodium benzoate	Fresh mango juice with 0.01% ZrMo	Fresh mango juice with 0.01% ZrMo/Chitosan	Fresh mango juice with 0.01% ZrMo/AlG
Total bacterial count	Zero time	7.7×10^3	3.1×10^3	3.8×10^3	2.2×10^3	2.1×10^3
	2	8.5×10^3	4.2×10^3	4.9×10^3	3.6×10^3	3.4×10^3
	4	9.7×10^3	7.0×10^3	7.8×10^3	6.8×10^3	6.5×10^3
	6	®	8.1×10^3	8.7×10^3	7.7×10^3	7.4×10^3
	8		®	®	8.8×10^3	8.7×10^3
	10				®	®
Psyhcrophilic bacteria	Zero time	2.5×10^2	1.0×10^2	1.2×10^2	0.3×10^2	0.2×10^2
	2	3.9×10^2	2.1×10^2	2.7×10^2	1.9×10^2	1.5×10^2
	4	7.1×10^2	4.0×10^2	4.2×10^2	3.1×10^2	3.0×10^2
	6	®	6.0×10^2	6.3×10^2	4.9×10^2	4.4×10^2
	8		®	®	6.3×10^2	6.0×10^2
	10				®	®
Spore-forming bacteria	Zero time	3.9×10^2	1.9×10^2	2.0×10^2	1.2×10^2	0.9×10^2
	2	5.6×10^2	3.9×10^2	4.0×10^2	2.3×10^2	2.1×10^2
	4	6.9×10^2	5.4×10^2	5.6×10^2	4.7×10^2	4.2×10^2
	6	®	6.5×10^2	6.6×10^2	5.4×10^2	5.3×10^2
	8		®	®	6.3×10^2	6.1×10^2
	10				®	®
Total molds & yeasts	Zero time	4.0×10^3	2.7×10^3	2.8×10^3	1.4×10^3	1.1×10^3
	2	5.6×10^3	4.5×10^3	4.7×10^3	3.7×10^3	3.2×10^3
	4	8.2×10^3	5.7×10^3	5.9×10^3	4.9×10^3	4.8×10^3
	6	®	7.8×10^3	7.9×10^3	5.9×10^3	5.7×10^3
	8		®	®	7.8×10^3	7.4×10^3
	10				®	®

®: At these point samples were rejected.

Table 3 Effect of feeding fresh mango juice treatments for 4 weeks on the body weight (g) in male albino rats.

Groups of rats feeding fresh mango juice	Time			
	1st week	2nd week	3rd week	4th week
Control	182.2 ± 16.93	207.8 ± 17.22	228.8 ± 15.87	242.6 ± 20.07
Fresh mango juice with 0.01% Sodium benzoate	182.6 ± 12.99	202.8 ± 22.37	224.8 ± 33.76	238.6 ± 36.59
Fresh mango juice with 0.01% ZrMo	182.0 ± 8.34	202.6 ± 14.33	222.6 ± 18.35	233.4 ± 20.60
Fresh mango juice with 0.01% ZrMo/Chitosan	182.8 ± 10.06	206 ± 13.02	228.4 ± 12.54	238.6 ± 12.97
Fresh mango juice with 0.01% ZrMo/AlG	183.2 ± 14.46	211.6 ± 27.40	238.6 ± 38.84	252 ± 43.98
L.S.D*$_{0.05}$	14.44	21.92	30.26	32.96

Values are means ± SD for 5 rats. Data were analyzed by one-way analysis of variance (ANOVA). F test Means ($p < 0.05$).
* Least significant differences.

3.8. Biological evaluation

Biological evaluation of feeding fresh mango juice with sodium benzoate, ZrMo, ZrMo/Chitosan and ZrMo/AlG for 4 weeks on the some biological parameters of male albino rats. The data concerning the body weight and the mean square values of the different experimental groups at weekly intervals are shown in Table 3 illustrated that, there were no significant differences between control and experimental diet (fresh mango juice with sodium benzoate, ZrMo, ZrMo/Chitosan and ZrMo/AlG) in rat body weights. These values ranged from 182.2 g in the first week to 242.6 g in the fourth week for control diet. While the body weights values of groups of rats received in their diet feeding on fresh mango juice with sodium benzoate, ZrMo, ZrMo/Chitosan and ZrMo/AlG ranged from 182.6 to 238.6 g., 182.0 to 233.4 g, 182.8 to 238.6 g and 183.2 to 252 g, respectively, during experimental duration (four weeks).

The relative weight of liver, kidney, spleen and heart are shown in Table 4 the results indicated that no clear trend for dietary treatment was observed. The weight of the liver, kid-

Table 4 Effect of feeding fresh mango juice treatments for 4 weeks on the relative organs weight of liver, kidney, spleen and heart in male albino rats.

Groups of rats feeding fresh mango juice	Relative organs weigh of male albino rats			
	Liver %	Kidney%	Spleen%	Heart %
Control	3.42 ± 0.69	0.95 ± 0.20	0.38 ± 0.18	0.35 ± 0.04
Fresh mango juice with 0.01% Sodium benzoate	3.43 ± 0.83	0.98 ± 0.23	0.50 ± 0.22	0.38 ± 0.10
Fresh mango juice with 0.01% ZrMo	3.75 ± 0.63	0.90 ± 0.14	0.51 ± 0.20	0.40 ± 0.07
Fresh mango juice with 0.01% ZrMo/Chitosan	3.67 ± 0.58	0.95 ± 0.08	0.52 ± 0.16	0.38 ± 0.04
Fresh mango juice with 0.01% ZrMo/AlG	3.51 ± 0.56	0.99 ± 0.13	0.48 ± 0.13	0.36 ± 0.04
L.S.D*$_{0.05}$	0.87	0.21	0.24	0.08

Values are means ± SD for 5 rats. Data were analyzed by one-way analysis of variance (ANOVA). F test Means ($p < 0.05$).
* Least significant differences.

Table 5 Effect of feeding fresh mango juice with sodium benzoate, ZrMo, ZrMo/Chitosan and ZrMo/AlG for 4 weeks on some biological parameters of male albino rats.

Biological parameters	Groups of rats feeding fresh mango juice					
	Control	Fresh mango juice with 0.01% Sodium benzoate	Fresh mango juice with 0.01% ZrMo	Fresh mango juice with 0.01% ZrMo/Chitosan	Fresh mango juice with 0.01% ZrMo/AlG	L.S.D*$_{0.05}$
Cholesterol (mg/dl)	59.00 ± 7.21	70.00 ± 6.56	68.67 ± 2.31	61.33 ± 9.29	74.00 ± 6.08	12.17
Triglycerides (mg/dl)	62.67 ± 11.55	56.33 ± 3.06	51.00 ± 6.08	58.00 ± 10.44	66.67 ± 11.02	16.47
HDL-C (mg/dl)	34.33 ± 5.51	34.00 ± 11.36	34.33 ± 2.08	31.00 ± 3.61	34.00 ± 12.12	14.64
LDL-C (mg/dl)	42.67 ± 4.51	49.00 ± 4.00	48.33 ± 2.52	43.67 ± 5.51	51.67 ± 4.04	7.69
Urea (mg/dl)	53.00 ± 10.54	51.00 ± 20.07	57.33 ± 8.50	52.33 ± 8.62	48.67 ± 7.37	21.75
Creatinine (mg/dl)	0.66 ± 0.06	0.73 ± 0.13	0.70 ± 0.03	0.61 ± 0.14	0.71 ± 0.05	0.17
GPT (ALT) U/L	10.67 ± 4.73	17.00 ± 14.00	12.67 ± 9.07	12.33 ± 1.15	8.67 ± 1.15	14.54
GOT (AST) U/L	11.67 ± 3.21	15.00 ± 6.24	14.33 ± 2.52	14.67 ± 4.16	13.67 ± 1.15	6.21

Values are means ± SD for 5 rats. Data were analyzed by one-way analysis of variance (ANOVA). F test Means ($p < 0.05$).
* Least significant differences.

ney, spleen and heart was unaffected by any adding of the 0.01% Sodium benzoate, 0.01% Zr Mo, 0.01% Zr Mo/Chitosan and 0.01% Zr Mo/AlG to the diet and there were no significant differences between control and all the other groups under investigation.

The effect of feeding fresh mango juice with sodium benzoate, ZrMo, ZrMo/Chitosan and ZrMo/AlG for 4 weeks on serum cholesterol (mg/dl), triglycerides (mg/dl), HDL-C (mg/dl), LDL-C (mg/dl), urea (mg/dl), creatinine (mg/dl), GPT (ALT)U/L and GOT (AST) U/L of rats are shown in Table 5. These results showed that no significant differences ($p < 0.05$) for these values between different investigated groups of rats feeding fresh mango juice with sodium benzoate, ZrMo, ZrMo/Chitosan and ZrMo/AlG for 4 weeks as well as control diet.

4. Conclusion

The outcome of this study may have a major impact on the development of novel nanomaterials for fresh mango juice safeguard engineering. The incorporation of $Zr(MoO_4)_2$ into chitosan or alginate hydrogel beads showed a safeguard toward the studied types of bacterial and fungi. The role of ZrMo or its hybrid products may be regarded from the view point of either increase formation of reactive oxygenated species (ROS) in the bead matrix that can interact with protein and/or due to their functional ionic groups (NH^{3+} and COO^{-}) which have a potential antimicrobial effect. These results provide important insights into the ability of fresh mango juice storage using new in-situ dispersed composites obtained via surface modification of ZrMo. This may be essential for promoting the application of such technique for fresh juice fruits preservation without big cost or expensive equipment and these additives also reduced microbial counts and improved fresh mango juice without any adverse changes on biological effects.

Declaration of Competing Interest

The authors declare that there is no conflict of interest for the following paper

Acknowledgements

The authors are grateful to Benha University and Hot Labs. Center, Atomic Energy Authority, Egypt. Also, Umm Al-Qura University, Makkah, Saudi Arabia, Ain Shams and Mansoura University, Egypt.

References

Ali, I.M., 2010. Synthesis and sorption properties of new synthesized rare-earth-doped sodium titanate. J. Radioanal. Nucl. Chem. 285, 263–270.

Ali, I.M., Zakaria, E.S., Khalil, M., El-tantawy, A., El-Saied, F.A., 2020. Efficient enrichment of Eu3 +, Tb3 +, La3 + and Sm3 + on a double core shell nano composite based silica. J. Inorg. Organomet. Polym Mater. 30, 1537–1552.

Allain, C.C., Poon, L.S., Chan, C.S., Richmond, W., Fu, P.C., 1974. Enzymatic determination of total serum cholesterol. Clin. Chem. 20, 470–475.

Aly, A.A., Refaey, M.M., Hameed, A.M., Sayqal, A., Abdella, S.A., Mohamed, A.S., Hussain, M.A.A., Ismail, H.A., 2020. Effect of addition sesame seeds powder with different ratio on microstructural and some properties of low fat Labneh. Arab. J. Chem. 13, 7572–7582.

AOAC, 1995. Official Methods of Analysis. Association of Official Analytical Chemists International,16th ed. Arlington, Virginia, USA

Blasse, G., Dirksen, G.J., 1987. Luminescence of high-temperature zirconium molybdate. J. Phys. Chem. Solids 48, 591–592.

Bui, T.H., Hong, S.P., Yoon, J., 2018. Development of nanoscale zirconium molybdate embedded anion exchange resin for selective removal of phosphate. Water Res. 134, 22–31.

Chen, K., Iglesia, E., Bell, A.T., 2001. Isotopic tracer studies of reaction pathways for propane oxidative dehydrogenation on molybdenum oxide catalysts. J. Phys. Chem. B 105, 646–653.

Chen, Y., Li, J., Li, Q., Shen, Y., Ge, Z., Zhang, W., Chen, S., 2016. Enhanced water-solubility, antibacterial activity and biocompatibility upon introducing sulfobetaine and quaternary ammonium to chitosan. Carbohydr. Polym. 143, 246–253.

Cheng, P., Zhou, Q., Hu, X., Su, S., Wang, X., Jin, M., Shui, L., Gao, X., Guan, Y., Nözel, R., Zhou, G., Zhang, Z., Liu, J., 2018. Transparent glass with the growth of pyramid-type MoS2 for highly efficient water disinfection under visible-light irradiation. ACS Appl. Mater. Interfaces 10, 23444–23450.

Chvapil, M., Chvapil, T.A., Owen, J.A., Keown, K., 1978. Reaction of vaginal tissue of rabbit and of cheek pouch of hamster to inserted collagen sponges treated with either zinc or copper. Am. J. Obstet. Gynecol. 130, 63–70.

Clearfield, A., Blessing, R.H., 1972. The preparation and crystal structure of a basic zirconium molybdate and its relationship to ion exchange gels. J. Inorg. Nucl. Chem. 34, 2643–2663.

El-Gammal, B., Ibrahim, G., El-Kholy, S.H., Shady, S.A., 2015. Ion-exchange equilibrium of cesium/hydrogen ions on zirconium molybdate and zirconium iodomolybdate cation exchangers. Desalin. Water Treat. 55, 2121–2143.

Fawcett, J.K., Scott, J.E., 1960. A rapid and precise method for the determination of urea. J. Clin. Pathol. 13, 156.

Friedewald, W.T., Levy, R.I., Fredrickson, D.S., 1972. Estimation of the concentration of low-density lipoprotein cholesterol in plasma, without use of the preparative ultracentrifuge. Clin. Chem. 18, 499–502.

Frings, C.S., Fendley, T.W., Dunn, R.T., Queen, C.A., 1972. Improved determination of total serum lipids by the sulfo-phospho-vanillin reaction. Clin. Chem. 18, 673–674.

Gallington, L.C., Chapman, K.W., Morelock, C.R., Chupas, P.J., Wilkinson, A.P., 2013. Orientational order-dependent thermal expansion and compressibility of ZrW2O8 and ZrMo2O8. Phys. Chem. Chem. Phys. 15, 19665–19672.

Gan, D., Xu, T., Xing, W., Ge, X., Fang, L., Wang, K., Ren, F., Lu, X., 2019. Mussel-inspired contact-active antibacterial hydrogel with high cell affinity, toughness, and recoverability. Adv. Funct. Mater. 29, 1805964.

Gordienko, M.G., Palchikova, V.V., Kalenov, S.V., Lebedev, E.A., Belov, A.A., Menshutina, N.V., 2020. The alginate–chitosan composite sponges with biogenic Ag nanoparticles produced by combining of cryostructuration, ionotropic gelation and ion replacement methods. Int. J. Polym. Mater. Polym. Biomater., 1–11.

Gupta, V.K., Agarwal, S., Tyagi, I., Pathania, D., Rathore, B.S., Sharma, G., 2015. Synthesis, characterization and analytical application of cellulose acetate-tin (IV) molybdate nanocomposite ion exchanger: binary separation of heavy metal ions and antimicrobial activity. Ionics 21, 2069–2078.

Hu, Z.-H., Omer, A.M., Ouyang, X.K., Yu, D., 2018. Fabrication of carboxylated cellulose nanocrystal/sodium alginate hydrogel beads for adsorption of Pb(II) from aqueous solution. Int. J. Biol. Macromol. 108, 149–157.

Hultberg, B., Andersson, A., Isaksson, A., 1997. Copper ions differ from other thiol reactive metal ions in their effects on the concentration and redox status of thiols in HeLa cell cultures. Toxicology 117, 89–97.

Ismail, H.A., Hameed, A.M., Refaey, M.M., Sayqal, A., Aly, A.A., 2020. Rheological, physio-chemical and organoleptic characteristics of ice cream enriched with Doum syrup and pomegranate peel. Arab. J. Chem. 13, 7346–7356.

Kulig, D., Zimoch-Korzycka, A., Jarmoluk, A., Marycz, K., 2016. Study on alginate-chitosan complex formed with different polymers ratio. Polymers 8.

Le, V., 1993. Development of alternative technologies for gel-type chromatographic 99mTc generators.

Li, M., Liu, X., Xu, Z., Yeung, K.W.K., Wu, S., 2016. Dopamine modified organic-inorganic hybrid coating for antimicrobial and osteogenesis. ACS Appl. Mater. Interfaces 8, 33972–33981.

Liu, H., Cheung, P., Iglesia, E., 2003. Zirconia-supported MoOx catalysts for the selective oxidation of dimethyl ether to formaldehyde: structure, redox properties, and reaction pathways. J. Phys. Chem. B 107, 4118–4127.

Monroy-Guzmán, F., Díaz-Archundia, L.V., Contreras Ramírez,, A., 2003. Effect of Zr: Mo ratio on 99mTc generator performance based on zirconium molybdate gels. Appl. Radiat. Isotopes 59, 27–34.

Pan, X., Wu, J., Zhang, W., Liu, J., Yang, X., Liao, X., Hu, X., Lao, F., 2021. Effects of sugar matrices on the release of key aroma compounds in fresh and high hydrostatic pressure processed Tainong mango juices. Food Chem. 338, 128117.

Patiño-Ruiz, D., Marrugo, L., Reyes, N., Acevedo-Morantes, M., Herrera, A., 2020. Ionotropic gelation synthesis of chitosan-alginate nanodisks for delivery system and *in vitro* assessment of prostate cancer cytotoxicity. Int. J. Polym. Sci. 2020, 5329747.

Pogrebnjak, A., Sukhodub, L., Sukhodub, L., Bondar, O., Kumeda, M., Shaimardanova, B., Shaimardanov, Z., Turlybekuly, A., 2019. Composite material with nanoscale architecture based on bioapatite, sodium alginate and ZnO microparticles. Ceram. Int. 45, 7504–7514.

Reitman, S., Frankel, S., 1957. A colorimetric method for the determination of serum glutamic oxalacetic and glutamic pyruvic transaminases. Am. J. Clin. Pathol. 28, 56–63.

Sæther, H.V., Holme, H.K., Maurstad, G., Smidsrød, O., Stokke, B. T., 2008. Polyelectrolyte complex formation using alginate and chitosan. Carbohydr. Polym. 74, 813–821.

Sahoo, P.P., Madras, S.S.G., Guru Row, T.N., 2009. Synthesis, characterization, and photocatalytic properties of ZrMo2O8. J. Phys. Chem. C 113, 10661–10666.

Salè, F.O., Marchesini, S., Fishman, P.H., Berra, B., 1984. A sensitive enzymatic assay for determination of cholesterol in lipid extracts. Anal. Biochem. 142, 347–350.

Schermer, S., Winsen, T.V., 1967. The Blood Morphology of Laboratory Animals. F. A. Davis Company, Philadelphia.

Sharma, S., Sanpui, P., Chattopadhyay, A., Ghosh, S.S., 2012. Fabrication of antibacterial silver nanoparticle—sodium alginate–chitosan composite films. RSC Adv. 2, 5837–5843.

Tamayo, L., Azócar, M., Kogan, M., Riveros, A., Páez, M., 2016. Copper-polymer nanocomposites: An excellent and cost-effective biocide for use on antibacterial surfaces. Mater. Sci. Eng., C 69, 1391–1409.

Thammitiyagodage, M.G., de Silva, N.R., Rathnayake, C., Karunakaran, R., Wgss, K., Gunatillka, M.M., Ekanayaka, N., Galhena, B.P., Thabrew, M.I., 2020. Biochemical and histopathological changes in Wistar rats after consumption of boiled and un-boiled water from high and low disease prevalent areas for chronic kidney disease of unknown etiology (CKDu) in north Central Province (NCP) and its comparison with low disease prevalent Colombo, Sri Lanka. BMC Nephrol. 21, 38.

Turlybekuly, A., Pogrebnjak, A.D., Sukhodub, L.F., Sukhodub, L.B., Kistaubayeva, A.S., Savitskaya, I.S., Shokatayeva, D.H., Bondar, O.V., Shaimardanov, Z.K., Plotnikov, S.V., Shaimardanova, B.H., Digel, I., 2019. Synthesis, characterization, in vitro biocompatibility and antibacterial properties study of nanocomposite materials based on hydroxyapatite-biphasic ZnO micro- and nanoparticles embedded in Alginate matrix. Mater. Sci. Eng., C 104, 109965.

Venkatesan, J., Lee, J.-Y., Kang, D.S., Anil, S., Kim, S.-K., Shim, M. S., Kim, D.G., 2017. Antimicrobial and anticancer activities of porous chitosan-alginate biosynthesized silver nanoparticles. Int. J. Biol. Macromol. 98, 515–525.

Yin, M., Lin, X., Ren, T., Li, Z., Ren, X., Huang, T.-S., 2018. Cytocompatible quaternized carboxymethyl chitosan/poly(vinyl alcohol) blend film loaded copper for antibacterial application. Int. J. Biol. Macromol. 120, 992–998.

Wahid, F., Wang, H.S., Zhong, C., Chu, L.Q., 2017. Facile fabrication of moldable antibacterial carboxymethyl chitosan supramolecular hydrogels cross-linked by metal ions complexation. Carbohydr. Polym. 165, 455–461.

Wahid, F., Zhong, C., Wang, H.-S., Hu, X.-H., Chu, L.-Q., 2017b. Recent advances in antimicrobial hydrogels containing metal ions and metals/metal oxide nanoparticles. Polymers 9.

Zakaria, E.S., Ali, I.M., Khalil, M., Mohamed, T.Y., El-Tantawy, A., 2016. Synthesis, characterization and isotherm studies of new composite sorbents. Bull. Mater. Sci. 39, 1709–1724.

Zhang, Y., Li, L., Su, H., Huang, W., Dong, X., 2015. Binary metal oxide: advanced energy storage materials in supercapacitors. J. Mater. Chem. A 3, 43–59.

Zhu, M., Liu, X., Tan, L., Cui, Z., Liang, Y., Li, Z., Kwok Yeung, K. W., Wu, S., 2020. Photo-responsive chitosan/Ag/MoS2 for rapid bacteria-killing. J. Hazard. Mater. 383, 121122.